A [Cyclentetrakis(methylene)]tetrakis[2-hydroxybenzamide] Ligand That Complexes and Sensitizes Lanthanide(III) Ions

Anthony D'Aléo,[1] Jide Xu,[1] King Do,[2] Gilles Muller,[2]

and Kenneth N. Raymond*[1]

1-Chemical Sciences Division, Lawrence Berkeley National Laboratories, Berkeley, California 94720, and Department of Chemistry, University of California, Berkeley, California 94720-1460.

2- Department of Chemistry, San José State University, San José, CA 95192-0101

raymond@socrates.berkeley.edu

Abstract

The synthesis of a cyclen derivative containing four isophthalamide groups (L^1) is described. The spectroscopic properties of the Ln(III) conplexes of L^1 (Ln= Gd, Tb, Yb, Eu) reveal changes of the UV/visible absorption, circular dichroism absorption, luminescence and circularly polarized luminescence properties. It is shown that at least two metal complex species are present in solution, whose relative amounts are pH dependent. When at pH > 8.0, an intense long lived emission is observed (for [L^1Tb] and [L^1Yb]) while at pH < 8.0, a weaker, shorter-lived species predominates. Unconventional Ln(III) emitters (Pr, Nd, Sm, Dy and Tm) were sensitized in basic solution, both in the visible and in the near infra-red, to measure the emission of these ions.

Introduction

Luminescent lanthanide complexes have attracted much recent attention because of their use and further potential in a wide variety of applications such as bio-fluoroimmunoassays,[1, 2] as sensors,[3-7] in light emitting diodes,[8-10] and as waveguide amplifiers for lasers.[11-18] In most of the cases, luminescent lanthanide complexes consist of a lanthanide ion attached to a chelating chromophore which transfers the excitation energy to the lanthanide ion, which must be protected from water coordination to avoid quenching. The presence of this chromophore overcomes the limitation of an intrinsically small molar absorption coefficient (ε) for the metal by using a strongly absorbing organic ligand. This light harvesting phenomenon is known as the *antenna effect*, and compared to the bare cations, increases the brightness (defined as the product of the luminescence quantum yield and of the molar absorption coefficient) and the luminescence lifetimes of the lanthanide ions, which are highly sensitive to the local environment and quenched by overtones of X-H vibrations, where X = O, N, C.

At the molecular level, the strong paramagnetism of these ions has led to important applications in NMR shift reagents applicable in 3D protein structure determination, for example.[19] The ligand field splitting of Ln(III) can also be used to determine changes in coordination geometry around the lanthanide ion.[20-24] In such cases, the luminescence pattern can be used to determine or indicate a change in the geometry of the binding atoms about

the lanthanide center. In addition, chiral ligands allow the use of techniques such as circular dichroism (CD) absorption or circular polarized luminescence (CPL) that provide insight into the chiral ligand conformations (number of species present as well as differentiation of those species).

We report herein the synthesis of a ligand ($\mathbf{L^1}$) composed of a cyclen scaffold with four appended isophthalamide (IAM) groups. $\mathbf{L^1}$ was complexed to a series of Ln(III) (Ln = Gd, Tb, Yb, Eu, Pr, Nd, Sm, Dy and Tm). A detailed study on the spectroscopic properties of the uncomplexes ligand as well as its Gd, Tb, Yb and Eu complexes shows the presence of two emissive species whose relative amounts depend on the pH of the base/buffer used. The dominant species at high pH luminesces intensely and exhibits a long luminescence lifetime, while the species dominant at mildly acidic pH is less emissive and has a shorter lifetime. Assignment of the emissive transitions for other, unconventional Ln(III) (Ln= Pr, Nd, Sm, Dy and Tm) is also presented.

Experimental Section

General

Thin-layer chromotography (TLC) was performed using precoated Kieselgel 60 F254 plates. Flash chromatography was performed using EM Science Silica Gel 60 (230- 400 mesh). NMR spectra were obtained using either Bruker AM-300 or DRX-500 spectrometers operating at 300 (75) MHz and 500 (125) MHz for ^{1}H (or ^{13}C) respectively. ^{1}H (or ^{13}C) chemical shifts are

reported in ppm relative to the solvent resonances, taken as δ7.26 (δ77.0) and δ2.49 (δ39.5) respectively for $CDCl_3$ and $(CD_3)_2SO$, while coupling constants (*J*) are reported in Hz. The following standard abbreviations are used for characterization of ^{1}H-NMR signals: s = singlet, d = doublet, t = triplet, q = quartet, quin = quintet, sext= sextet, m = multiplet, dd = doublet of doublets and br= broad. Fast-atom bombardment mass spectra (FABMS) were performed using 3-nitrobenzyl alcohol (NBA) or thioglycerol/glycerol (TG/G) as the matrix. Elemental analyses were performed by the Microanalytical Laboratory, University of California, Berkeley, CA.

Synthesis

Methyl 2-methoxy-3-methylbenzoate (1)

To a mixture of 3-methyl-salicylic acid (200 g, 1.32 mol), anhydrous potassium carbonate (500 g, 3.6 mol) and dry acetone (3.5 L) in a 5 L round bottom flask, dimethylsulfate (210 mL, 2.2 mol) was added in several portions. The mixture was stirred for 2 days (the reaction monitored by TLC) and then heated at reflux overnight,. The reaction mixture was then filtered, and the filtrate was evaporated to remove the solvents; a pale yellow thick oil was obtained as the product, yield 215 g, 91%; ^{1}H-NMR (500 MHz, $CDCl_3$, 25 ºC): 2.26 (s, 3H, C*H*$_3$), 3.782 (s, 3H, OC*H*$_3$), 3.85 (s, 3H, OC*H*$_3$), 6.98 (t, ^3J = 7.5 Hz, 1H, Ar*H*), 7.27 (d, ^3J = 7.5 Hz, 1H, Ar*H*), 7.58 (d, ^3J = 7.5 Hz, 1H, Ar*H*); ^{13}C-NMR (125 MHz, $CDCl_3$, 25 ºC): 15.7, 51.8, 61.2, 123.3, 124.4, 128.9, 132.5, 134.88, 158.2, 166.6.

3-Bromomethyl-2-methoxy-benzoic acid methyl ester (2)

In a 500 mL 2 necks round bottom flask, fitted with a reflux condenser and a dropping funnel, were placed 0.05 mol of methyl 2-methoxy-3-methylbenzoate and 80 mL of benzene. A 1000-watt halogen-tungsten lamp was place in an upright position about 3 cm from the flask. The solution was gently refluxed while 0.05 mol of bromine in 80 mL of benzene was added at such a rate that a red color persisted at all times. The reaction was judged complete when all the bromine was added and the red bromine color had disappeared. 92%; ^{1}H-NMR (500 MHz, $CDCl_3$, 25 ºC): 3.92 (s, 3H, OC*H*$_3$), 3.96 (s, 3H, OC*H*$_3$), 4.58 (s, 2H, BrC*H*$_2$), 6.86 (t, ^{3}J= 7.8 Hz, 1H, Ar*H*), 7.55 (dd, ^{3}J= 7.5, 1.8 Hz, 1H, Ar*H*), 7.81 (dd, ^{3}J= 7.5, ^{4}J= 1.8 Hz, 1H, Ar*H*); ^{13}C-NMR (125 MHz, $CDCl_3$, 25 ºC): 27.4, 52.3, 62.8, 123.9, 124.7, 132.4, 132.8, 135.19, 158.5, 166.1.

1,4,7,10-tetrakis(2-methoxy-3-carboxybenzyl)-1,4,7,10-tetraazacyclododecane tetramethyl ester (3)

To a solution of cyclen (300 mg, 1.74 mmol) in 30 mL of dry acetonitrile were added of 3.1 mL N,N'-diisopropylethylamine (18 mmol) and **2** (2.1 g, 8.1 mmol) consecutively. The reaction mixture was warmed to 60 °C under nitrogen for 24 hours. The white precipitate was filtered, washed with 3 x 5 mL of actonitrile and dried in vacuo, giving a beige solid. 81%; ^{1}H-NMR (500 MHz, $CDCl_3$, 25 ºC): 2.73 (s, 16H, cyclen-*H*), 3.55 (s, 8H, benzylC*H*$_2$), 3.72 (s, 12H, OC*H*$_3$), 3.98 (s, 12H, OC*H*$_3$), 6.87 (t, ^{3}J= 7.5 Hz, 4H, Ar*H*), 7.63 (d, ^{3}J= 7.5 Hz, 4H, Ar*H*), 7.91 (d, ^{3}J= 7.5 Hz, 4H, Ar*H*); ^{13}C-NMR (125 MHz, $CDCl_3$, 25 ºC): 52.1, 53.2, 53.5, 62.0, 123.4, 123.9,

134.3, 134.5, 158.2, 166.7; (+)-FABMS: *m/z*: 885.5 [MH^+] for. $C_{48}H_{60}N_4O_{12}$ Exact Mass: 884.42.

1,4,7,10-tetrakis(2-methoxy-3-carboxybenzyl)-1,4,7,10-tetraazacyclododecane (4)

To a stirred solution of **3** (445 mg, 0.5 mmol) in 30 mL of methanol was added of 10% aqueous KOH solution (1 mL). The reaction mixture was stirred for 16 hours. The volatiles were removed under reduced pressure and the residue was dissolved in water. The solution was neutralized with 6 N HCl , the product was collected as beige solid. **4** was dried in vacuo, giving a beige solid. 91%; ^{1}H-NMR (300 MHz, D_2O-NaOD, 25 ºC) : 2.80 (br, s, 8H, cyclen-C*H*$_2$), 3.67 (s, 12H, methoxy C*H*$_2$), 2.75 (br,s, 8H, benzylC*H*$_2$), 7.15 (t, ^3J= 7.2 Hz, 4H, Ar*H*), 7.51 (d, ^3J= 6.9 Hz, 4H, Ar*H*), 7.65 (d, ^3J= 7.2 Hz, 4H, Ar*H*), 13.04 (br,s, 4H, acid *H*); (+)-FABMS: *m/z*: 773 [MH^+] for. $C_{40}H_{44}N_4O_{12}$ Exact Mass: 772.3.

1,4,7,10-tetrakis(2-methoxy-3-(1-R-(+)-phenyl-ethylcarbamoyl)-benzyl)-1,4,7,10-tetraazacyclododecane (5)

To a stirred solution of **4** (77 mg, 1 mmol) in dry DMF (5 mL), the solution was cooled in an ice bath, R-(+)-methylbenzyl amine (0.5 mL, 4.1 mmol)) was added under nitrogen. The cold mixture was treated with HATU (O-(7-azabenzotriazol-1-yl)-N, N,N',N'-tetramethyluronium hexafluorophosphate, 0.77 g, 2 mmol) and diisopropylethyl-amine (1 mL, 5.7 mmol) successively. The mixture was stirred 7 h and the solvent was removed under reduced pressure. The residue was partitioned between CH_2Cl_2 (20 mL) and 1M HCl (2 x 20 mL). The organic phase was purified by flash chromatography

over flash silica gel eluting with a gradient of 3-7% MeOH in CH_2Cl_2. The appropriate fractions were collected and evaporated to dryness to give **5** as white foam, yield 71%. ^{1}H-NMR (300 MHz, $CDCl_3$, 25 ºC) : 1.56 (s, 12H, CH_3), 2,83 (br, s, 16H, cyclen-C*H*$_2$), 3.46 (s, 12H, C*H*$_3$O), 3.65 (s, 8H, C*H*$_2$), 7.03 (t, ^3J= 8.0 Hz, 4H, Ar*H*), 7.20-7.40 (m, 20H, Ar*H*), 7.48 (d, ^3J= 8.1 Hz, 4H, Ar*H*), 7.84 (d, ^3J= 7.8 Hz, 4H, Ar*H*); ^{13}C-NMR (125 MHz, $CDCl_3$, 25 ºC): 21.2, 39.4,49.7, 51.2, 62.4, 124.2, 125.9, 127.1, 128.4, 128.8, 131.2, 134.1, 142.9, 156.5, 164.1, 170.4; (+)-FABMS: *m/z*: 1241.6 [MH^+] for $C_{76}H_{88}N_8O_8$ Exact Mass: 1240.67.

1,4,7,10-tetrakis(2-methoxy-3-(1-phenyl-ethylcarbamoyl)-benzyl)-1,4,7,10-tetraazacyclododecane (L^1)

To a stirred solution of **5** (445 mg, 0.5 mmol) in 30 mL of dry dichloromethane was added an excess of BBr_3 (1 mL) with cooling under nitrogen. The reaction mixture was stirred for 48 hours. The volatiles were removed under reduced pressure and the residue was quenched with methanol (150 mL). The methanol solution was refluxed gently in an open round bottom flask overnight. The methanol solution was then boiled with water for 6 hours, the product precipitated as a beige solid upon cooling and was dried in vacuo, giving **L^1** , yield 85%. ^{1}H-NMR (300 MHz, $CDCl_3$, 25 ºC): 1.46 (s, 12H, C*H*$_3$), 2,80-3.30 (br, s, 16H, cyclen C*H*$_2$), 3.98 (s, 8H, C*H*$_2$), 5.18 (m, 4H, chiral C*H*), 6.18 (t, ^3J= 7.5 Hz, 1H, Ar*H*), 6.99 (t, ^3J= 8.5 Hz, 3H, Ar*H*), 7.20-7.40 (m, 20H, Ar*H*), 7.58 (d, ^3J= 7.2 Hz, 4H, Amide*H*), 7.95 (d, ^3J= 8.1 Hz, 1H, Ar*H*), 8.09 (d, ^3J= 7.8 Hz, 3H, Ar*H*). 9.20 (d, ^3J= 7.8 Hz, 1H, Ar*H*), 9.29 (d, ^3J= 8.4 Hz, 3H, Ar*H*); (+)-FABMS:

m/z: 1185.6 [MH^+] for $C_{72}H_{80}N_8O_8$ Exact Mass: 1184.61; Anal. Calc.(found) For $C_{72}H_{80}N_8O_8 \cdot 2HBr$: C, 64.19 (64.23), H, 6.13 (6.43), N, 8.32 (8.14).

Synthesis of Cyclene-TetraIAM lanthanide pyridinium complex

In a 25mL round bottom flask, Cyclene-TetraIAM (1Eq) was dissolved in 3mL of methanol with three drops of pyridine. Lanthanide(III) chloride hexahydrate (1Eq) in 3mL of methanol was added. The solution was heated to reflux temperature during 4hours, and then left to cool to room temperature. Slow evaporation of the methanol at room temperature for one night afforded a precipitate of the complex, which was collected by filtration.

[L^1Gd]Br_2: 17%; Anal. Calc.(found) For $C_{81}H_{90}N_9O_8Gd \cdot 2HBr \cdot 9H_2O$: C, 51.98 (51.98), H, 5.88 (5.57), N, 6.74 (6.84).

[L^1Tb]Br_2: 23%; Anal. Calc.(found) For $C_{81}H_{90}N_9O_8Tb \cdot 2HBr \cdot 9H_2O$: C, 51.96 (52.07), H, 5.81 (5.98), N, 6.73 (6.71).

[L^1Yb]Br_2: 22%; Anal. Calc.(found) For $C_{81}H_{90}N_9O_8Yb \cdot 2HBr \cdot 15H_2O$: C, 48.38 (48.09), H, 6.16 (5.99), N, 6.27 (6.33).

Optical spectroscopy

UV-Visible absorption spectra were recorded on a Varian Cary 300 double beam absorption spectrometer. Circular dichroism spectra were measured with a JASCO J-810 spectrapolarimeter. Circularly polarized luminescence and total luminescence spectra were recorded on an instrument described previously,[25, 26] operating in a differential photon-counting mode. The light

source for indirect excitation was a continuous wave 450 W xenon arc lamp from a Spex FluoroLog-2 spectrofluorometer, equipped with excitation and emission monochromators with dispersions of 4 nm/mm (SPEX, 1681B). Selective excitation of Tb(III) was accomplished with either a Coherent Innova-70 or Coherent Sabre TSM 15. The optical detection system consisted of a focusing lens, long pass filter, and 0.22 m monochromator. The emitted light was detected by a cooled EMI-9558B photomultiplier tube operating in photon-counting mode. All measurements were performed with quartz cuvettes with a path length of 0.4 or 1.0 cm. Emission spectra were acquired on a HORIBA Jobin Yvon IBH FluoroLog-3 spectrofluorimeter, equipped with 3 slit double grating excitation and emission monochromators (2.1 nm/mm dispersion, 1200 grooves/mm). Spectra were reference corrected for both the excitation light source variation (lamp and grating) and the emission spectral response (detector and grating). Luminescence lifetimes were determined on a HORIBA Jobin Yvon IBH FluoroLog-3 spectrofluorimeter, adapted for time-correlated single photon counting (TCSPC) and multichannel scaling (MCS) measurements. A sub-microsecond Xenon flashlamp (Jobin Yvon, 5000XeF) was used as the light source, with an input pulse energy (100 nF discharge capacitance) of *ca*. 50 mJ, yielding an optical pulse duration of less than 300 ns at FWHM. Spectral selection was achieved by passage through the same double grating excitation monochromator. Emission was monitored perpendicular to the excitation pulse, again with spectral selection achieved by passage through the double grating emission monochromator (2.1 nm/mm dispersion, 1200

grooves/mm). A thermoelectrically cooled single photon detection module (HORIBA Jobin Yvon IBH, TBX-04-D) incorporating fast rise time PMT, wide bandwidth preamplifier and picosecond constant fraction discriminator was used as the detector. Signals were acquired using an IBH DataStation Hub photon counting module and data analysis was performed using the commercially available DAS 6 decay analysis software package from HORIBA Jobin Yvon IBH. Goodness of fit was assessed by minimizing the reduced chi squared function, χ^2, and a visual inspection of the weighted residuals. Each trace contained at least 10,000 points and the reported lifetime values resulted from at least three independent measurements. Typical sample concentrations for both absorption and fluorescence measurements were *ca*. 10^{-5}-10^{-6} M and 1.0 cm cells in quartz suprasil or equivalent were used for all measurements. Quantum yields were determined by the optically dilute method (with optical density <0.1) using the following equation;

$$\Phi x/\Phi r = [Ar(\lambda r)/Ax(\lambda x)][I(\lambda r)/I(\lambda x)][nx2/nr2][Dx/Dr]$$

where *A* is the absorbance at the excitation wavelength (λ), *I* is the intensity of the excitation light at the same wavelength, *n* is the refractive index and *D* is the integrated luminescence intensity. The subscripts '*x*' and '*r*' refer to the sample and reference respectively. For quantum yield calculations, an excitation wavelength of 340 nm was utilized for both the reference and sample, hence the *I(λr)/I(λx)* term is removed. Similarly, the refractive indices term, *nx2/nr2*, was taken to be identical for the aqueous reference and sample solutions. Hence, a plot of integrated emission intensity (*i.e. Dr*)

vs. absorbance at 340 nm (*i.e. Ar(λr)*) yields a linear plot with a slope which can be equated to the reference quantum yield Φ*r*. Quinine sulfate in 0.5 M (1.0 *N*) sulfuric acid was used as the reference ($\Phi_r = 0.546$). By analogy, for the sample, a plot of integrated emission intensity (*i.e. Dx*) versus absorbance at 340 nm (*i.e. Ax(λx)*) yields a linear plot and Φ*x* can then be evaluated. The values reported in the manuscript are the average of four independent measurements. For Yb(III), since there is no reliable NIR reference, the luminescence quantum yield were measured one respectively to the other fixing, arbitrary, the value of the lowest pH measured to 1.

Synthesis

The ligand was synthesized by a six-step synthesis starting from commercially available 3-methyl-salicylic acid (**1**). First, the phenolic and carboxylic acid were protected by methyl groups (**2**) using dimethylsulfide. Subsequently, the tolyl group was oxidized to give the methylene bromide derivative (**3**). This synthon readily reacted with cyclen in basic medium yielding **4**. This protected ester was then saponified (**5**) and the chiral amine group was introduced by amidation using HATU (**6**). Finally, the phenolic methyl ether functions were deprotected using BBr_3 yielding the desired ligand in rather good yield (32% overall).

The metal complexes were prepared using an excess of pyridine as base by refluxing one equivalent of ligand with one equivalent of $LnCl_3 \cdot 6H_2O$ in methanol for 12 hours. The resultant complexes were precipitated by adding diethyl ether, washed thoroughly with pentane and cold diethyl ether, and

dried before submission to elemental analysis. All complexes analyzed fit with a **$[L^1LnH_3]Br_2$** complex formula with the bromide counterion introduced from the ligand deprotection strategy. The ytterbium complex of **L^2** was made *in situ* by adding 0.5 Eq of $YbCl_3 \cdot 6H_2O$ in methanol solution as described for Tb(III) derivatives.[22] The full characterization of the ligands and complexes and synthetic details are reported in the experimental section.

The ligand **L^1** contains twelve coordinating atoms (four oxygen atoms from IAM phenolate, four carbonyl groups from IAM and the four nitrogen atoms from the cyclen backbone), and possesses eight distinct pK_a values (four belonging to the cyclen scaffold and four belonging to the IAM phenol/phenolate). In the presence of lanthanide ions, **L^1** is expected to form ML complexes with a coordination number of eight (CN = 8) as confirmed by elemental analysis of the isolated lanthanide complexes. Furthermore, the presence of sterically hindered groups on the amide side of the IAM can be usefull in order to protect the metal center from the local environement.

Results and discussion

Since the complexes were not stable in aqueous solution, the spectroscopic properties of **L^1**, **$[GdL^1]$**, **$[TbL^1]$**, **$[YbL^1]$** and **$[EuL^1]$** were carried out in methanol solution where the stability was found to be higher. In order to control the basicity of the methanol solutions, different organic bases with their known pK_a values were used.

1. Ligand

The UV/visible absorption spectra of the ligand using various bases with p*K*as ranging from 0.2 to 14.0 are plotted in Figure 1a, whereas the data are reported in Table 1. As can be seen, the molar absorption coefficients vary from 19,000 to 23,500 $M^{-1}\cdot cm^{-1}$ and are in good agreement with those of $\mathbf{[(L^2)_2Tb]^-}$ (19,300-26,500 $M^{-1}\cdot cm^{-1}$).[22] This is consistent with the four IAM units branched on the cyclen moiety. Of special importance is that the absorption maximum is blue-shifted from 335 nm in highly basic media (pH from 8.3 to 14.0) to 305 nm (pH below 6.0) with an isosbestic point around 320 nm. By plotting the pH dependence of the molar absorption coefficients at 305 and 335 nm (Figure 1b), one can see the presence of a long transition between 4.8 and 11.2, which strongly suggests the presence of numerous protonations of $\mathbf{L^1}$.

The luminescence spectra of $\mathbf{L^1}$ were measured in methanol solutions. The quantum yields were determined using quinine bisulfate in 1N sulphuric acid as the standard and corrected for the different refractive indexes of the solvents.[27] Selected spectra are shown in Figure S1a and all the data are reported in Table 1. In acidic medium, only one broad emission band is observed, with a maximum around 435 nm. This emission maximum is red-shifted compared to the maximum observed in the absorption spectra (100-130 nm Stoke shift). In basic medium the same emission profile is observed, with a shoulder on the blue side of the emission. This shoulder can be attributed to the emission band of the singlet excited state (with a small Stokes shift), while the main emission band around 435 nm corresponds to the triplet excited state of $\mathbf{L^1}$. It should be noted that the observation of the

unconventional emission from the triplet excited state at room temperature is due to the heavy atom effect induced by the bromide salt of the ligand. This was confirmed by recording the emission spectra at 77 K (Figure S2).

2. Gadolinium

Trivalent gadolinium ion was chosen because of its similar electronic structure and size with europium ($4f^7$ versus $4f^6$), but lacking an accessible metal-based low energy electronic excited state (the lowest one, $^6P_{7/2}$, lies at 32,224 cm^{-1}). As a result, one can expect the same kind of information found for the free ligand but it will correspond to the positions of the excited singlet and triplet states of the ligand complexed to the Gd(III) cation. For instance, the molar absorption coefficients range between 19,000 and 23,500 $M^{-1}\cdot cm^{-1}$, whereas the absorption maxima are found between 305 and 325 nm in basic medium, with an isosbestic point at 313 nm (Figure S3a). These changes in the position of the absorption maxima between the free and complexed ligands confirm the formation of the complex.

The complex formation is also corroborated by the changes observed in the pH dependence of the UV/visible absorption molar coefficient values (Figure S3b). Unlike the free ligand (one protonation step, Figure S1b), the complexation of $\mathbf{L^1}$ to Gd(III) showed two different protonation steps, observed between 4-5 and 7-8, respectively. In addition to the isosbestic point at 313 nm, there is also one at 341 nm that can be associated to the higher pH species.

As observed for the ligand, the emission spectra of **[L^1Gd]** are dependent on the pH determined by the bases used (Figure S4a). The main difference between $\mathbf{L^1}$ and its Gd(III) complex was that the emission spectrum has a broad emission band around 375 nm, corresponding to the singlet excited state, with a shoulder growing in at 435 nm (attributed to the triplet excited state) when the pH is decreased. It should be noted that the variation of the quantum yield cannot be taken into account since two different states are involved and the intersystem crossing rate changes with the conditions (Figure S4b).

At 77 K, despite a small residual emission arising from the singlet excited state, the emission spectra are mainly composed of a structured emission band located around 430 nm. The deconvolution of this triplet excited state emission band into a vibronic progression[28-30] of several overlapping Gaussian functions with separations of *ca*. 1000-1100 cm^{-1} led to the determination of a value of 24,690 cm^{-1} for the triplet excited state energy. Such a high energy triplet excited state should allow sensitization of many lanthanide ions, including Eu(III), Tb(III), Pr(III), Nd(III), Sm(III), Dy(III), or Tm(III) (*vide infra*).

Finally, it must be emphasized that the Gd(III) complex is unstable under acidic conditions, since identical absorption spectra and molar absorption coefficient values (within the experimental errors) were obtained for $\mathbf{L^1}$ and its gadolinium(III) complex at room temperature (see Tables 1 and 2). A similar observation was noticed for the emission spectra recorded at 77 K (the two emission bands broaden to give similar spectra than for $\mathbf{L^1}$).

3. Terbium

Since the $^5D_4$ level is at 20,500cm^{-1} (Tb(III) emitting excited state) and its next excited state ($^5G_6$) is 6,000 cm^{-1} higher, terbium appears to be the ideal lanthanide to be sensitized by **L^1**, based on the good match between the Tb(III) and triplet excited state energies. The photophysical and chiroptical properties of **[L^{1}Tb]** were studied by UV/visible absorption, CD absorption, luminescence (luminescence quantum yield and luminescence lifetimes), and CPL spectroscopies at various pH values between 2.8 and 14.0. All the results are summarized in Table 3 and selected spectra are presented hereafter.

The UV/visible profile of **[L^{1}Tb]** is identical to the one of **[L^{1}Gd]** with a shift of the absorption maximum from 305 nm to 325 nm when going from acidic to basic conditions (Figure 3a). The molar absorption coefficient values are around 20,000 M^{-1}·cm^{-1}, as observed for **L^1** and **[L^{1}Gd]**. As for **[L^{1}Gd]**, the UV/visible spectra of **[L^{1}Tb]** show two isosbestic points and the pH dependence of the molar absorption coefficient values reveals the presence of two different p*K*as (between 4-5 and around 7-8). The photophysical properties of the Gd(III) and Tb(III) complexes are then in good agreement, and, more importantly, three species are present in solution. The change between these species seems to occur with pH values between 4-5 and 7-8.

As shown in Figure 3b, the luminescence spectra of **[L^{1}Tb]** are different, depending on the base used and resultant pH. In basic medium, the typical luminescence spectrum of terbium ion can be observed with sharp line emission bands arising from the $^5D_4$ excited state on the ^7F_J manifold ground state. In an acidic medium, only the triplet excited state luminescence band can be observed, which suggests that the complex is not formed under these conditions. This is confirmed by the observation of the terbium- and ligand-centered emissions in the luminescence spectra of **[L^{1}Tb]** under mild basic conditions (pH of 5-6).

The luminescence quantum yield of the terbium complex can be calculated and separated from that of the triplet excited state. Thus the dependence of the quantum yield of both excited states as a function of the pH of the base buffers used can be followed (Figures 4c and 4d). In the case of the Tb-centered emission, one can see that the luminescence quantum yield is low (3-4%) at low pH. A considerable increase is observed at pH ~ 4-5 (14-20%) and continues until it reaches its maximum (~60%). On the other hand, the opposite effect can be observed when looking at the triplet excited state emission (*i.e.* large and low quantum yields in acidic and basic media, respectively). This quenching of the triplet excited state emission as the Tb-centered luminescence increases reflects the efficiency of the energy transfer (poor and good efficiencies in acidic and basic conditions, respectively) and that the separation of these two species is possible when using bases of appropriate strength.

This luminescence study allows us to conclude that there are at least two different species depending on the pH of the solution, resulting in changes in the emission efficiency.

Another way to observe the number of species is to measure the luminescence lifetime of the Tb-centered emission. At room temperature, one monoexponential decay around 2.1 ms can be found above pH ~ 6, while below this pH, a second component can be detected with a shorter luminescence lifetime around 800 μs (Figure S5a and Table 3). The intensity of the latter emission decreases by increasing the pH as the long-lived, deprotonated species dominates the species distribution.

Measurements in deuterated solvent enable calculation of "*q*" the number of inner sphere bound solvent molecules.[31] These experiments were performed using piperidine, triethylamine, pyridine and 3-hydroxypyridine as buffer bases in d^4-methanol and showed a monoexponential decay with identical luminescence lifetimes at high pH (using piperidine and triethylamine) and at lower pH (using pyridine and 3-hydroxypyridine). Application of Beeby's equation[32] to methanol gave 0.0 and 0.3 inner sphere water molecules (the latter value reflects the protonation of a nearby atom in the complexing ligand when decreasing the pH). This result establishes that there is no methanol molecule in the inner sphere of the Tb(III) complexes.

Since $\mathbf{L^1}$ and its complexes are chiral, CD absorption spectra were measured. As shown in Figure 5a, different spectra were obtained,

depending on the pH. In basic medium, the CD spectra revealed two CD exciton bands located at 310 and 335 nm, with positive and negative values, respectively. At neutral pH, the CD spectra only show one main CD exciton band at 335 nm with a positive value. It is interesting to note that, in the case of acetic acid or trifluoroacetic acid, a different pattern can be seen with a residual "complex" absorption at 335 nm for acetic acid, while with trifluoroacetic acid (pH = 0.2), no remaining transition can be observed at this wavelength (Figure 5a). In addition, the pH dependence of the Δdeg also suggests the presence of two different species (pH around 7-8).

Also, measurements of circularly polarized luminescence (CPL to study the chiroptical properties of the Tb(III)-containing compound) has been performed. Generally speaking, CPL spectroscopy is the emission analog to CD absorption spectroscopy. CD allows one to detect the differential absorption of left and right circularly polarized lights, while CPL measures the difference in the emission intensity of left and right circularly polarized light. With Tb(III) complexes, the studied transition is the magnetic dipole allowed transition, $^5D_4 \rightarrow {}^7F_5$, where one predicts the CPL would be large.[33] In such measurements, the luminescence dissymmetry ratio, g_{lum}, is defined as follows:

$$g_{lum} = \frac{\Delta I}{\frac{1}{2} I} = \frac{I_L - I_R}{\frac{1}{2}\left(I_L + I_R\right)}$$

where I_L and I_R refer, respectively, to the intensity of left and right circularly polarized lights.

As can be seen from Figure 6, the CPL spectra of the magnetic dipole allowed transition, $^5D_4 \rightarrow {}^7F_5$ of **[L^{1}Tb]**, display several peaks corresponding to crystal-field splitting of the electronic level.

However, differences in the magnitude, sign and shape of the CPL signals indicate that the chiral structure of the Tb(III) complex is dependent of the nature of the base present in solution (Figure 6). It is interesting to note that the CPL activity exhibited by the **[L^{1}Tb]** complex in the presence of triethylamine is comparable when either a direct excitation of the Tb(III) ion (λ_{exc} = 488 nm) or an indirect excitation through the ligand absorption bands (λ_{exc} = 331 nm) is used (Table 4). Observation of similar CPL spectra following direct and indirect excitations indicates that the same species in solution is responsible for the CPL activity detected.[26] A useful experiment to determine whether or not the solution contains a mixture of species is to excite directly the Tb(III) ion with circularly polarized light. These experiments have shown that the g_{lum} values obtained for **[L^{1}Tb]** in methanol solution in the presence of triethylamine were independent of the polarization of the excitation beam (*i.e.* right-, left-, or plane-polarized light). This is consistent with the presence of only one species in solution. If the solution would have contained a mixture of diastereomers or enantiomers, the CPL should have been dependent on the excitation polarization.[26]

On the other hand, the g_{lum} values obtained for the **[L^{1}Tb]** complex solution in the presence of pyridine were dependent of the polarization of the

excitation beam. In addition, different g_{lum} values were obtained when a direct excitation of the Tb(III) ion (λ_{exc} = 488 nm) and an indirect excitation through the ligand absorption bands (λ_{exc} = 330 nm) were used (Table 4). These results would suggest that the solution of the **[L^{1}Tb]** complex contains more than one species responsible for the CPL activity measured when the solution is prepared with pyridine as a base. This is confirmed by the observation of two different CPL spectra when direct and indirect excitations are used (Figure 6b).

4. Ytterbium

Luminescence experiments were also performed using Yb(III) ion. Ytterbium is interesting since it is a near infra-red (NIR) emitter which possesses only one excited state ($^2F_{5/2}$). Because of the latter point, the luminescence quantum yield is relatively high for a lanthanide ion emitting in the NIR, thus making the measurement easier than for other NIR emitters. Indeed, the energy gap between the triplet excited state and $^2F_{5/2}$ is large (ΔE= 14,290 cm^{-1}) which makes the energy transfer much less efficient than for the visible emitters. On the other hand, the absence of excited states between the triplet and $^2F_{5/2}$ avoids any back transfer deactivation pathway. The UV/visible absorption spectra are identical to the ones of the Tb(III) and Gd(III) complexes when using piperidine or 3-hydroxypyridine.

As can be seen in Figure 7a, in the most basic conditions (piperidine), the emission is composed of mainly four splittings between 950 and 1150 nm with the most intense at 997 nm. Using a less basic base such as 3-

hydroxypyridine (Figure 7b), a strikingly different spectrum is obtained with the first splitting as the dominant one (at 975 nm). The spectrum obtained using the latter condition leads to the "usual" ytterbium emission as often reported for Yb-based compounds.[34-38] It should be indicated that the profile of the emission spectrum shown in Figure 7a was already observed for phosphor[39] and also in glass or solid state.[34, 40] This suggests an important change of the geometry around the metal as the crystal field changes.

The dependence of the visible luminescence quantum yield and the ytterbium emission area as a function of the pH (Table 5 and Figure 13) were investigated as for the Tb(III) complex. In the visible region of the spectrum (Figure 13a), it can be seen that there is a considerable decrease in luminescence quantum yield at pH > 7.4. Unfortunately, the study of the sensitization process with Yb(III) is precluded due to the changes observed in the emission profile (emission shifting from the triplet excited state to the singlet excited state bands). The same phenomenon was observed for the Gd(III) complex (observation of the emission from the singlet and triplet excite states when basic and acidic conditions were used, see Table 2). However, the NIR relative luminescence quantum yield trend (slight increase until 7.4 followed by a considerable jump and then again a slightly increase until reaching a plateau, Figure S6) clearly supports the presence of two species that certainly possess different geometries around the metal. This hypothesis is also corroborated by the important emission pattern change observed in the Yb-centered luminescence spectra. It was also

confirmed by the pH dependence of the luminescence lifetime of the ytterbium in the NIR (Figure 7b and Table 5). As for the Tb(III) complex, a monoexponential decay is observed in basic conditions, whereas two lifetimes can be found when the pH is lower than 7.0. This clearly shows the presence of a second species in solution.

To understand the striking difference of emission patterns, the Yb(III) complex of $\mathbf{L^2}$ was prepared. As can be seen in Figure 8, the emission of $\mathbf{[(L^2)_2Yb]^-}$ is composed of a main splitting at 977 nm followed by a broad shoulder (much less intense). This emission profile looks like the emission of $\mathbf{[L^1Yb]}$ using 3-hydroxypyridine as a base. This suggests that at low pH, the complex existing in solution is based on the IAM units (no involvement of the cyclen unit) while, at high pH, the different spectrum seems to indicate that not only the IAM moiety but all or part of the cyclen moiety would participate to the complexation.

To ensure that the result is not just coincidencial, measurements in methanol (d^4, d^1 and d^0) were performed and all the results are reported in Table 6. As already discussed, the decay found for $\mathbf{[L^1Yb]}$ is biexponential using 3-hydroxypyridine as a base with a component around 2 μs and another one around 1 μs in methanol (d^0). The longer luminescence lifetime possesses a small weight as compared to the other one. It can also be found that the value of the relative luminescence quantum yield is identical (within the experimental error) to the one of $\mathbf{[L^1Yb]}$ using piperidine as a base. Interestingly, the shorter luminescence lifetime (1 μs) is close to that of $\mathbf{[(L^2)_2Yb]^-}$ (Table 6). In methanol d^1 and d^4 the same kind of trend can be

found. These results seem to confirm the fact that the complex formed mainly involved the IAM chromophore at low pH, whereas stronger bases certainly allow involvement of the cylcen moiety in lanthanide coordination. Thus, this yields different properties than for the "pure" IAM-based complexes.

The number of methanol molecules in the inner sphere (*n*) can be calculated using the formula developed for Yb(III) by Beeby *et al*.[41] adapted to methanol. This formula was defined in water using different kinds of ligand. Since the measurements were made in water, no C-H vibrations are brought by the solvent and, in consequence, this kind of vibration has not been taken into account. For **[L^{1}Yb]**, it can be found that, in piperidine, the complex does not have any solvent molecules in the inner sphere, while, at lower pH, the calculation suggests that there would be one molecule of solvent bound to the metal (n = 0.8) which is in contradiction with the data obtained for **[L^{1}Tb]**. This result certainly reflects the larger influence of the medium (OH, NH and CH vibrations) on the luminescence properties for Yb-based emission *vs.* Tb-based emission (visible emitter).

5. Europium

A reasonable level of sensitization was expected with Eu(III) because the triplet excited state is higher than the $^5D_2$ state (too high to be optimum).[42, 43] Instead, as illustrated in Figure 9a, only the triplet excited state emission

could be recorded. Therefore at 77 K, the "typical" and characteristically split spectrum of europium was observed (Figure 9).

The recovery of the sensitization occurring at 77 K strongly suggests that there is a transfer-back transfer interaction between the triplet excited state of the ligand and the $^5D_2$ of Eu(III) ion with a much faster triplet excited state relaxation (radiative and non radiative) than the $^5D_2 \rightarrow {}^5D_0$ relaxation.

At 77 K in solid matrix, a thorough study of the basicity dependence reveals two different patterns if one examines the J = 0 and J = 1 transitions (Figure 9b). Interestingly, only one J = 0 transition can be seen in all conditions, suggesting the presence of only one species. Also, no spectral differences are observed at pH higher or lower than 5.8, again suggesting the presence of only one species. Noticeably, luminescence lifetime experiment at 77 K confirmed the presence of only one species in every case: at high pH, a luminescence lifetime of 720 μs can be observed while in mildly basic conditions, a luminescence lifetime of 650 μs is measured.

These experiments on **[L^{1}Eu]** also prove the presence of two emissive species: one existing at high pH while the other one is present at pH lower than 7. In the following part, the best conditions of sensitization were used to sensitize other lanthanide ions.

6. Pr, Nd, Sm, Dy, Tm

Because the ligand triplet excited state energy seems well suited to populate most of the Ln(III) cations, all the lanthanide complexes emitting from the *f*-

f orbitals were prepared, yielding sensitization of Pr, Nd, Sm, Dy and Tm. With the exception of neodymium, which only possesses transitions in the NIR region, all these lanthanide ions emit in both the NIR and visible regions. All the relevant luminescence spectra in the visible and in the NIR regions are presented in Figure 10 and a brief description of these luminescence spectra is provided below.

For praseodymium, the $^3P_0$ (21,750 cm^{-1}) is populated yielding transitions attributed to the $^1D_2 \rightarrow {}^3H_4$ (Figure 10a), $^1D_2 \rightarrow {}^3F_3$ and $^1D_2 \rightarrow {}^3F_4$ (Figure 10b).

Neodymium is also sensitized by this ligand resulting in the typical emission feature of this ion (Figure S7) with the $^4F_{3/2} \rightarrow {}^4I_{11/2}$ and $^4F_{3/2} \rightarrow {}^4I_{13/2}$ transitions in the NIR.

For samarium, the $^4G_{5/2}$ excited state emits in the visible (Figure 10c) and in the NIR region where three transitions can be observed (Figure 10d), and arising from the $^4G_{5/2}$ level to the $^6F_{5/2}$, $^6F_{7/2}$ and $^6F_{9/2}$, respectively.

Dysprosium emits from the $^4F_{9/2}$ excited state giving rise to four transitions to the $^6H_{15/2}$, $^6H_{13/2}$, $^6H_{11/2}$, and $^6H_{9/2}/{}^6F_{11/2}$ in the visible (Figure 10e) and three transitions in the NIR (Figure 10f) attributed to the $^4F_{9/2} \rightarrow {}^7F_{7/2}$, $^4F_{9/2} \rightarrow {}^7F_{5/2}$ and $^4F_{9/2} \rightarrow {}^7F_{3/2}$.

Thulium emission from the $^1G_4$ level is observed with the $^1G_4 \rightarrow {}^3H_6$ and the $^1G_4 \rightarrow {}^3H_4$ transitions in the visible (Figure 10g) and the $^1G_4 \rightarrow {}^3F_4$ in the NIR (Figure 10h).

Conclusions

In conclusion, the synthesis of a cyclen derivative containing four isophthalamide groups ($\mathbf{L^1}$) is described. The spectroscopic properties of the Ln(III) conplexes of $\mathbf{L^1}$ (Ln= Gd, Tb, Yb, Eu) were studied and reveal that at least two species are present in solution whose relative populations are dependent on the pH. In basic medium, an intense long lived emission is observed (for **[$\mathbf{L^1}$Tb]** and **[$\mathbf{L^1}$Yb]**), while in mildly basic medium a weaker, shorter lived species is present. A study of the J = 0 and J = 1 transition patterns of **[$\mathbf{L^1}$Eu]** emission also supports the change in species upon protonation of the complexing ligand. These two different complexes change their coordination geometry upon protonation/deprotonation of one of the twelve coordinating atoms (eight oxygen and four nitrogen atoms), but in both cases still exclude solvent molecules from the inner coordination sphere. This was also supported by the lifetime and CPL measurements on some of the Ln(III) complexes of interest.

In addition, in the more basic conditions (the most efficient conditions for sensitization of Tb(III) and Yb(III)), other lanthanide ions (Pr(III), Nd(III), Sm(III), Dy(III) and Tm(III)) were sensitized showing emission in the near infra-red region (and in the visible in some cases). All emissive transitions on the spectra were attributed.

Acknowledgement

This work was partially supported by the NIH (Grant HL69832) and supported by the Director, Office of Science, Office of Basic Energy Sciences, and the Division of Chemical Sciences, Geosciences, and Biosciences of the U.S. Department of Energy at LBNL under Contract No. DE-AC02-05CH11231. This technology is licensed to Lumiphore, Inc. in which some of the authors have a financial interest. G.M. thanks the National Institute of Health Minority Biomedical Research Support (2 S06 GM008192-27) and the Henry Dreyfus Teacher-Scholar Award for financial support.

References

[1] H. L. Handl, R. J. Gillies, *Life Sci.* **2005**, *77*, 361.

[2] S. Petoud, S. M. Cohen, J.-C. G. Bünzli, K. N. Raymond, *J. Am. Chem. Soc.* **2003**, *125*, 13324.

[3] B. Song, G. Wang, M. Tan, J. Yuan, *J. Am. Chem. Soc.* **2006**, *128*, 13442.

[4] S. M. Borisov, O. S. Wolbeis, *Anal. Chem.* **2006**, *78*, 5094.

[5] M. I. Stich, S. Nagl, O. S. Wolbeis, U. Henne, M. Schaeferling, *Adv. Funct. Mater.* **2008**, *18*, 1399.

[6] D. Parker, *Coord. Chem. Rev.* **2000**, *205*, 109.

[7] M. S. Tremblay, M. Halim, D. Sames, *J. Am. Chem. Soc.* **2007**, *129*, 7570.

[8] J. Kido, Y. Okamoto, *Chem. Rev.* **2002**, *102*, 2357.

[9] T.-S. Kang, B. S. Harrison, T. J. Foley, A. S. Knefely, J. M. Boncella, J. R. Reynolds, K. S. Schanze, *Adv. Mater.* **2003**, *15*, 1093.

[10] A. De Betancourt-Dias, *Dalton Trans.* **2007**, 2229.

[11] K. Kuriki, Y. Koike, Y. Okamoto, *Chem. Rev.* **2002**, *102*, 2347.

[12] H. K. Kim, S. G. Roh, K.-S. Hong, J.-W. Ka, N. S. Baek, J. B. Oh, M. K. Nah, Y. H. Cha, J. Ko, *Macromol. Res.* **2003**, *11*, 133.

[13] B. Julian-Lopez, J. Planelles-Arago, E. Cordoncillo, B. Viana, C. Sanchez, *J. Mater. Chem.* **2008**, *18*, 23.

[14] J. K. R. Weber, J. J. Felten, B. Cho, P. C. Nordine, *Nature* **1998**, *393*, 769.

[15] L. H. Slooff, A. Polman, S. I. Klink, G. A. Hebbink, L. Grave, C. J. M. van Veggel, D. N. Reinhoudt, J. W. Hofstraat, *Opt. Mater.* **2000**, *14*, 101.

[16] L. H. Slooff, A. V. Blaaderen, A. Polman, G. A. Hebbink, S. I. Klink, C. J. M. van Veggel, D. N. Reinhoudt, J. W. Hofstraat, *J. Appl. Phys.* **2002**, *91*, 3955.

[17] S. Moynihan, R. Van Deun, K. Binnemans, J. Krueger, G. von Papen, A. Kewell, G. Crean, G. Redmond, *Opt. Mater.* **2007**, *29*, 1798.

[18] P. Escribano, B. Julian-Lopez, J. Planelles-Arago, E. Cordoncillo, B. Viana, C. Sanchez, *J. Mater. Chem.* **2008**, *18*, 23.

[19] G. Pintacuda, M. John, X.-C. Su, G. Otting, *Acc. Chem. Res.* **2007**, *40*, 206–212.

[20] W. G. Perkins, G. A. Crosby, *J. Chem. Phys.* **1965**, *42*, 407.

[21] W. G. Perkins, G. A. Crosby, *J. Chem. Phys.* **1965**, *42*, 2621.

[22] A. P. S. Samuel, J. Xu, K. N. Raymond, *Inorg. Chem.* **2009**, *48*, 687.

[23] A. Beeby, L. M. Bushby, D. Maffeo, J. A. G. Williams, *J. Chem. Soc. Dalton Trans* **2002**, 48.

[24] M. H. V. Werts, R. T. F. Jukes, J. W. Verhoeven, *Phys. Chem. Chem. Phys.* **2002**, *4*, 1542.

[25] S. D. Bonsall, M. Houcheime, D. A. Straus, G. Muller, *Chem. Commun.* **2007**, 3676.

[26] K. Do, F. C. Muller, G. Muller, *J. Phys. Chem. A* **2008**, *112*, 6789.

[27] J. N. Demas, G. A. Crosby, *J. Phys. Chem.* **1971**, *75*, 991–1024.

[28] E. G. Moore, J. Xu, C. J. Jocher, E. J. Werner, K. N. Raymond, *J. Am. Chem. Soc.* **2006**, *128*, 10648

[29] E. G. Moore, J. Xu, C. J. Jocher, I. Castro-Rodriguez, K. N. Raymond, *Inorg. Chem.* **2008**, *47*, 3105.

[30] A. D'Aléo, J. Xu, E. G. Moore, C. J. Jocher, K. N. Raymond, *Inorg. Chem.* **2008**, *47*, 6109.

[31] R. C. Holz, C. A. Chang, W. D. Horrocks, *Inorg. Chem.* **1991**, *30*, 3270.

[32] A. Beeby, I. M. Clarkson, R. S. Dickins, S. Faulkner, D. Parker, A. S. d. Sousa, J. A. G. Williams, M. Woods, *J. Chem. Soc. Perkin Trans. 2* **1999**, 493.

[33] J. P. Riehl, G. Muller, *Handbook on the Physics and Chemistry of Rare Earths*, Gschneidner, K.A., Bünzli, J.-C.G., Pecharsky, V.K. ed., North-Holland Publishing, Amsterdam, **2005**.

[34] J. X. Meng, K. F. Li, J. Yuan, W. K. Wong, K. W. Cheah, *Chem. Phys. Lett.* **2000**, *332*, 313.

[35] S. Faulkner, A. Beeby, M.-C. Carriéa, A. Dadabhoya, K. A. M., P. G. Sammesa, *Inorg. Chem. Communication* **2001**, *4*, 187.

[36] A. Beeby, R. S. Dickins, S. Faulkner, P. D., J. A. G. Williams, *Chem. Commun.* **1997**, 1401.

[37] N. M. Shavaleev, L. P. Moorcraft, S. J. A. Pope, Z. R. Bell, S. Faulkner, M. D. Ward, *Chem. Eur. J.* **2003**, *9*, 5283.

[38] G. S. Kottas, M. Mehlstaubl, R. Frohlich, L. De Cola, *Eur. J. Inorg. Chem.* **2007**, 3465.

[39] W. Ryba-Romanowski, S. Golab, *J. Mol. Struct.* **1998**, *450*, 223.

[40] J. Le Person, V. Nazabal, R. Balda, J.-L. Adam, J. Fernandez, *Opt. Mater.* **2005**, *27*, 1748.

[41] S. Faulkner, A. Beeby, R. S. Dickins, D. Parker, J. A. G. Williams.

[42] M. Latva, H. Takalob, V.-M. Mukkala, C. Matachescuc, J. C. Rodriguez-Ubisd, J. Kankarea, *J. Lumin.* **1997**, *75*, 149.

[43] A. D'Aléo, A. Picot, A. Beeby, J. A. G. Williams, B. Le Guennic, C. Andraud, O. Maury, *Inorg. Chem.* **2008**, *47*, 10258.

Table 1. Optical properties of $\mathbf{L^1}$ in methanol at RT and at 77 K using different bases.

Table 2. Optical properties of L^1Gd in methanol at RT and at 77 K using different bases.

Table 3. Optical properties of **[$\mathbf{L^1Tb}$]** in methanol at RT and at 77 K.

Table 4. summary of the CPL data for **[$\mathbf{L^1Tb}$]** in methanol solutions.

Table 5. Photophysical properties of the **[$\mathbf{L^1Yb}$]** in methanol with O.D.= 0.11 optical density.

Table 6. Luminescence lifetime of **[$\mathbf{L^1Yb}$]** emission in methanol (d^4, d^1 and d^0)

Chart 1. Representation of the studied molecule and its model.

Scheme 1. Synthesis scheme for the preparation of the ligand.

Figure 1. a/ UV/visible absorption spectra of $\mathbf{L^1}$ as a function of the p*K*a of the base used [trifluoroacetic acid (—), chloroacetic acid (—), pyridine (—), triisopropanolamine (—), *sym*-collidine (—), triethylamine (—), piperidine (—)]; b/ Evolution of the UV/visible absorption molar absorption coeficient of $\mathbf{L^1}$ in methanol at 306 nm (■) and 335nm (●) as a function of the p*K*a of the base used.

Figure 2. Luminescence spectra of **[$\mathbf{L^1Gd}$]** in solid matrix (77 K in a mixture methanol/ethanol 1/4) with selected bases or acids (λ_{ex}= 320 nm). [piperidine (—), triethylamine (—), morpholine (—), sym-collidine (—)].

Figure 3. a/ UV/visible absorption spectra of **[L^{1}Tb]** in methanol as a function of the p*K*a of the base used; b/ Luminescence spectra of **[L^{1}Tb]** in methanol as a function of the p*K*a of the base used (λ_{ex}= 320 nm) [piperidine (—), triethylamine (—), morpholine (—), sym-collidine (—), 2-methylimidazol (—), triisopropanolamine (—), benzimidazol (—), pyridine (—), 3-hydroxypyridine (—), acetic acid (—), chloroacetic acid (—), trifluoroacetic acid (—)].

Figure 4. a/ Evolution of the UV/visible molar absorption coefficient for **[L^{1}Tb]** in methanol at 306 nm (■) and 325 nm (●) as a function of the p*K*a of the base used; b/ Evolution of the luminescence quantum yield for **[L^{1}Tb]** as a function of the p*K*a of the base used (only based on terbium emission).[■ aprotic "bases"; ● protic acids];c/ Evolution of the phosphorescence quantum yield for **[L^{1}Tb]** as a function of the p*K*a of the base used (only based on residual triplet emission).[■ aprotic; ● protic].

Figure 5. a/ CD absorption spectra of **[L^{1}Tb]** in methanol as a function of the p*K*a of the base used [piperidine (—), triethylamine (—), morpholine (—), sym-collidine (—), 2-methylimidazol (—), triisopropanolamine (—), imidazol (—), benzimidazol (—), pyridine (—), 3-hydroxypyridine (—), acetic acid (—),trifluoroacetic acid (—)]; b/ Evolution of the difference of molar absorption coefficient of **[L^{1}Tb]** in methanol at 336 nm as a function of the p*K*a of the base used.

Figure 6. a/ Circularly polarized luminescence (upper curve) and total luminescence (lower curve) spectra of the $^5D_4 \rightarrow {}^7F_5$ transition of the **[L^{1}Tb]**

complex in a 2.45 x 10^{-5} MeOH solution (OD = 0.6335) with 1% of triethylamine at 295 K, upon excitation at 331 or 488 nm. b/ Circularly polarized luminescence (upper curves) and total luminescence (lower curves) spectra of the $^5D_4 \rightarrow {}^7F_5$ transition of the **[L^{1}Tb]** complex in a 2.45 x 10^{-5} MeOH solution (OD = 0.589) with 1% of pyridine at 295 K, upon excitation at 330 (black) and 488 nm (green), respectively.

Figure 7. a/ Luminescence spectra of the **[L^{1}Yb]** complex in methanol in presence of piperidine in the NIR at RT (—) and at 77 K (—); b/ of the **[L^{1}Yb]** complex in methanol in presence of 3-hydroxypyridine in the NIR at RT (—) and at 77 K (—).(λ_{ex}= 340 nm); c/ Evolution of the luminescence quantum yield in the visible and of the luminescence relative intensity in the NIR in methanol as a function of the p*K*a of the base used for **[L^{1}Yb]**; d/ Evolution of the luminescence excited state lifetime for **[L^{1}Yb]** as a function of the p*K*a of the base used.

Figure 8. Luminescence spectrum of **[L^{1}Yb]** with piperidine as a base (—), **[L^{1}Yb]** with 3-hydroxypyridine as a base (—) and using **[(L^2)$_2$Yb]$^-$** with piperidine or 3-hydroxypyridine as a base (—) (λ_{ex}= 320 nm).

Figure 9. a/ Luminescence spectrum of **[L^{1}Eu]** in the visible in methanol containing 1% of piperidine at room temperature (λ_{ex}= 340 nm) (—) and at 77 K (λ_{ex}= 320 nm) (—); b/ Focus on the J= 0 et J=1 of the luminescence spectrum of **[L^{1}Eu]** in the visible in methanol/ethanol (1/4) at 77 K containing 1% of piperidine (—), of triethylamine (—), of morpholine (—), of

sym-Collidine (—), of imidazol (—), of pyridine (—) and of 3-Hydroxypyridine (—) (λ_{ex}= 320 nm).

Figure 10. Luminescence spectrum in methanol containing 1% of piperidine of a/ **[L^{1}Pr]** in the visible; b/ **[L^{1}Pr]** in the NIR; c/ **[L^{1}Sm]** in the visible; d/ **[L^{1}Sm]** in the NIR; e/ **[L^{1}Dy]** in the visible; f/ **[L^{1}Dy]** in the NIR; g/ **[L^{1}Tm]** in the visible; h/ **[L^{1}Tm]** in the NIR (λ_{ex}= 340 nm).

Table 1.

		S_1			T_1		77 K
Acid/base	pK_a	λ^{abs} (nm) / ε ($M^{-1}.cm^{-1}$)	λ^{em} (nm)	ϕ^{em}	λ^{em} (nm)	ϕ^{em}	λ^{em} (nm)
TFA	0.2	307 / 23,240	-[b]	-[b]	434	0.152	-[a], 422
ClAcOH	2.9	307 / 22,490	-[b]	-[b]	433	0.163	-[a], 428
MeOAcOH	3.5	308 / 18,940	-[b]	-[b]	430	0.149	361, 417
AcOH	4.8	307 / 22,440	-[b]	-[b]	434	0.225 (0.243)	361, 417
Pyridine	5.2	307 / 19,300	-[b]	-[b]	-[b]	0.097	-[a]
$N(iPrOH)_3$	5.9	310 / 16,830	-[b]	-[b]	437	0.113	373, 427
Sym-Collidine	7.4	334 / 19,830	-[b]	-[b]	436	0.108	362, 429
Morpholine	8.4	334 / 20,780	385[c]	-[c]	430	0.100	378, 421
$N(Et)_3$	9.8	335 / 20,570	386[c]	-[c]	422	0.224	385, 420
Piperidine	11.2	336 / 20,820	411	-[c]	-[b]	0.234	378, -[a]
TBAOH	14.0	335 / 23,620	408	-[c]	-[b]	0.315	N/A

a: undeterminable; b : no signal observed ; c: appears as a shoulder

Table 2.

		S_1			T_1		77 K
Acid/Base	pK_a	λ^{abs} (nm) / ε ($M^{-1}.cm^{-1}$)	λ^{em} (nm)	ϕ^{em}	λ^{em} (nm)	ϕ^{em}	λ^{em} (nm)
TFA	0.2	307 / 20,050	-[b]	-[b]	434	0.337	N/A
ClAcOH	2.9	307 / 19,900	-[b]	-[b]	432	0.336	-[b], 431
MeOAcOH	3.5	308 / 19,400	387[c]	-[b]	430	0.301	-[c], 429
AcOH	4.8	314 / 16,750	-[b]	-[b]	431	0.151 (0.139)	-[b], 431
Pyridine	5.2	317 / 17,800	374	-[b]	428[c]	0.055 (0.059)	374, 435
$N(iPrOH)_3$	5.9	321 / 19,300	374	-[b]	428[c]	0.022	375, 428
Sym-Collidine	7.4	323 / 18,600	371	-[b]	432	0.020 (0.025)	373, 431
Morpholine	8.4	324 / 21,900	377	-[b]	-[c]	0.021 (0.19)	377, -[b]
$N(Et)_3$	9.8	324 / 21,800	376	-[b]	-[c]	0.023 (0.025)	375, -[b]
Piperidine	11.2	325 / 22,000	374	-[b]	-[c]	0.020 (0.022)	374, -[c]
TBAOH	14.0	328 / 21,950		-[b]	-[c]	0.323	373, -[b]

a: undeterminable; b : no signal observed ; c: appears as a shoulder

Table 3.

			Ln			T1		77 K
	pK_a	λ^{abs} (nm)	λ^{em}	ϕ^{em}	τ^{em}	λ^{em}	ϕ^{em}	τ^{em}
Acid/Base		ε $M^{-1}.cm^{-1}$	nm		ms	nm		ms
TFA	0.2	307 / 19,820	-[b]	-[b]	-[b]	434	0.374	-[b]
Iminodiacetonitrile	2.8	310 / 21,010		0.025	2.08, 0.80	434	0.059	2.07, 0.73
ClAcOH	2.9	306 / 22,080	541	-[b]	2.06, 0.86	434	0.376	-[b]
MeOAcOH	3.5	301 / 23,260	541	-[b]	-[b]	434	0.059	2.05, 1.51
Benzoic acid	4.2	308 / N/A	541	0.036	2.08, 0.96	434	0.349	2.08, 0.58
AcOH	4.8	316 / 18,400	541	0.138	2.10, 0.96	434	0.062	2.05, 1.08
3-Hydroxypyridine	4.9	323 / 22,180	541	0.151	2.04, 0.81	434	0.060	2.09, 0.76
Pyridine	5.2	315 / 24,080	541	0.215	2.15; 0.86	434	0.071	2.05, 1.16
Benzimidazol	5.4	322 / 22030	541	0.301	2.03, 0.83	435	0.064	2.16, 0.93
Imidazol	5.8	321 / N/A	541	0.571	2.01	-[b]	-[b]	2.04
$N(iPrOH)_3$	5.9	322 / 20,380	541	0.541	2.11	-[b]	-[b]	2.11
2-Methylimidazol	7.0	326 / N/A	541	0.570	2.01	-[b]	-[b]	2.05
Sym-Collidine	7.4	325 / 22,570	541	0.535	2.12	-[b]	-[b]	2.08
Morpholine	8.4	325 / 24,390	541	0.540	2.10	-[b]	-[b]	2.08
N-Methyl diethanolamine	8.5	324 / 25,190		0.569	1.99	-[b]	-[b]	2.09
Diethanolamine	8.9	325 / 25,740		0.579	2.02	-[b]	-[b]	2.06
$N(Et)_3$	9.8	325 / 25,880	541	0.537	2.10	-[b]	-[b]	2.08
2-Methoxyethylamine	9.9	327 / N/A	541	0.581	2.00	-[b]	-[b]	2.05
Iminobispropylamine	10.7	325 / N/A	541	0.569	2.06	-[b]	-[b]	2.10
Piperidine	11.2	325 / 25,540	541	0.521	2.07	-[b]	-[b]	2.08
TBAOH	14.0	326 / 24,370	541	0.536	2.05	-[b]	-[b]	2.10

a: undeterminable; b : no signal observed ; c: appears as a shoulder

Table 4.

Complex	Electronic transition	λ / nm	g_{lum}	Solvent
L^1Tb	$^5D_4 \rightarrow {}^7F_5$	542.0	+0.045	MeOH / 1%
(λ_{exc} = 331 or 488 nm)		543.0	-0.053	triethylamine
L^1Tb	$^5D_4 \rightarrow {}^7F_5$	542.4	+0.043	MeOH / 1%
(λ_{exc} = 330 nm)		544.2	-0.062	pyridine
L^1Tb	$^5D_4 \rightarrow {}^7F_5$	543.2	+0.051	MeOH / 1%
(λ_{exc} = 488 nm)		549.2	-0.051	pyridine

Table 5.

Buffer	p*K*a	$\phi(^3T)$	Efficiency Yb	τ (μs)^{Yb}
3-Hydroxypyridine	4.9	0.048	1	2.1 ; 1.0
Pyridine	5.2	0.046	1.5	2.1 ; 0.93
Benzimidazol	5.4	0.047	1.7	2.1 ; 0.91
Imidazol	5.8	0.049	1.85	2.2 ; 0.86
$N(iPrOH)_3$	5.9	0.045	1.9	2.1 ; 0.98
2-Methylimidazol	7.0	0.015	2.1	2.3
Sym-Collidine	7.4	0.0042	5.2	2.1
Morpholine	8.4	0.0019	5.4	2.1
$N(Et)_3$	9.8	0.0015	5.7	2.1
Piperidine	11.2	0.0017	5.5	2.3

Table 6.

	CH_3OH	CH_3OD	CD_3OD
	τ (μs)	τ (μs)	τ (μs)
$[L^1Yb]$ (piperidine)	2.15	5.90	6.65
$[L^1Yb]$ (3-hydroxypyridine)	2.30 ; 1.05	5.80 ; 13.90	6.60 ; 17.10
$[(L^2)_2Yb]^-$	1.00	12.90	21.40

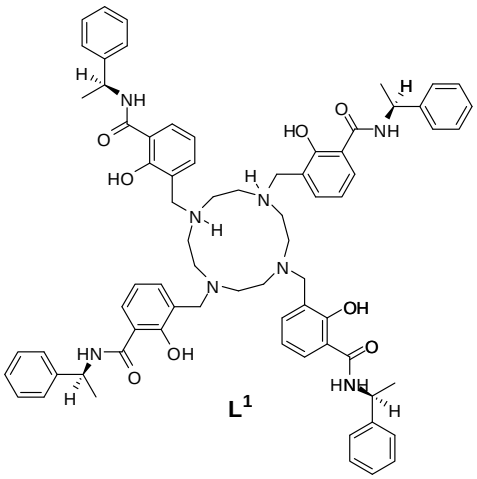

L^1

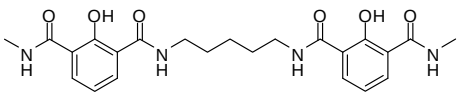

L^2

Chart 1.

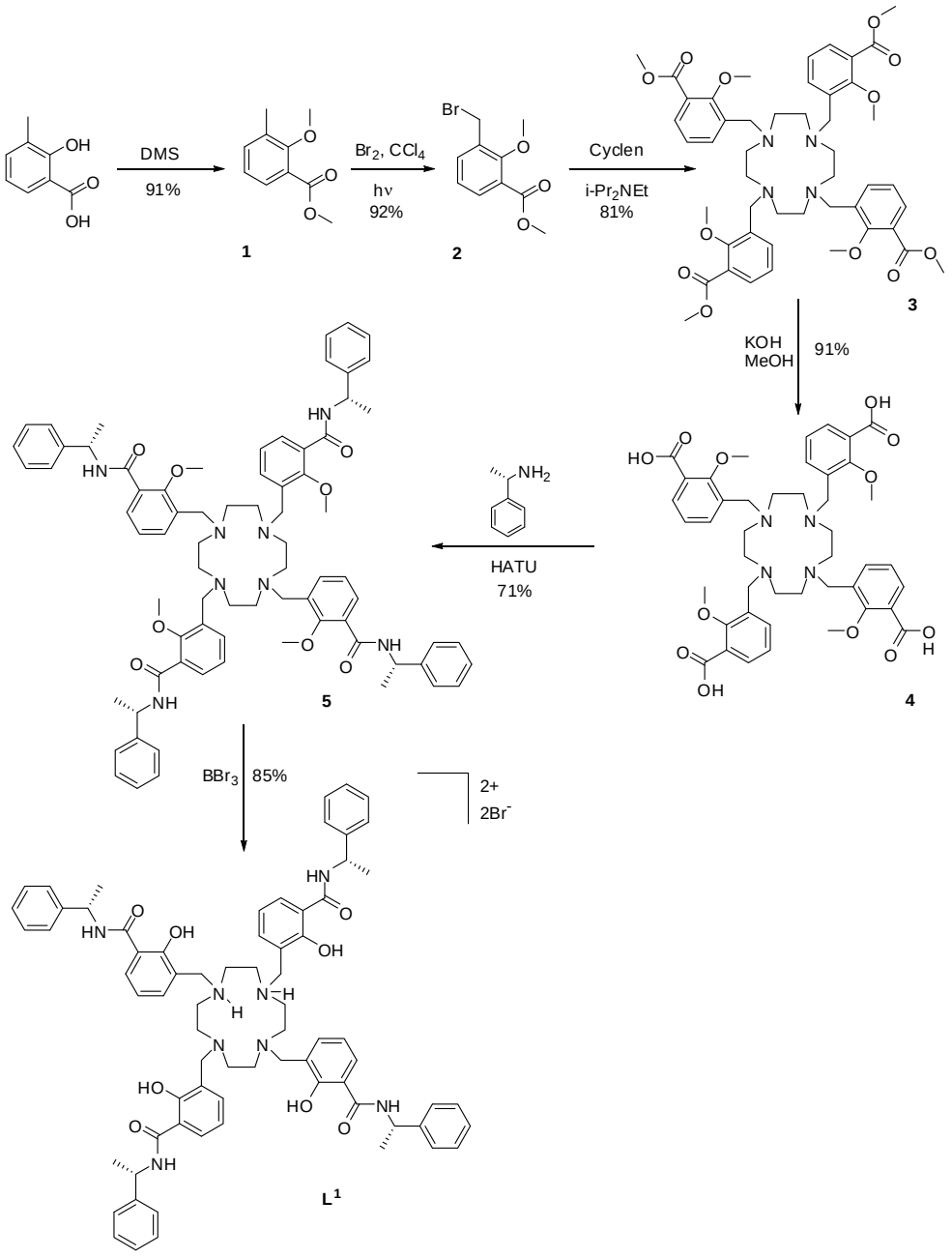
DMS
91%
Br2, CCl4
hν
92%
Cyclen
i-Pr2NEt
81%
KOH
MeOH
91%
HATU
71%
BBr3
85%
2+
2Br-
1
2
3
4
5
L1

Scheme 1.

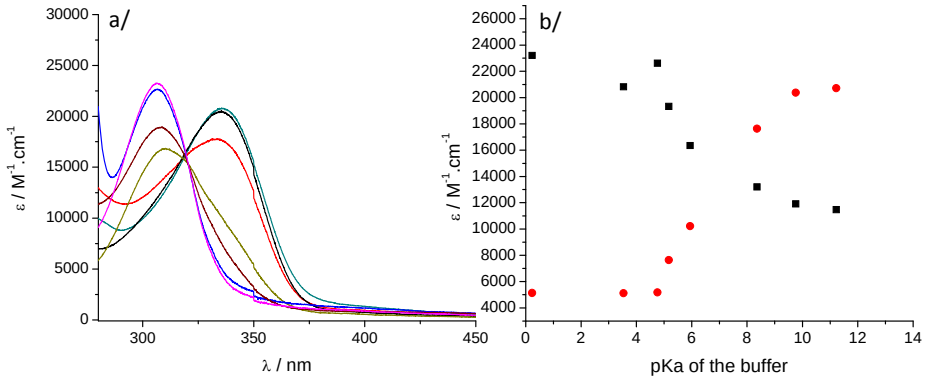

Figure 1.

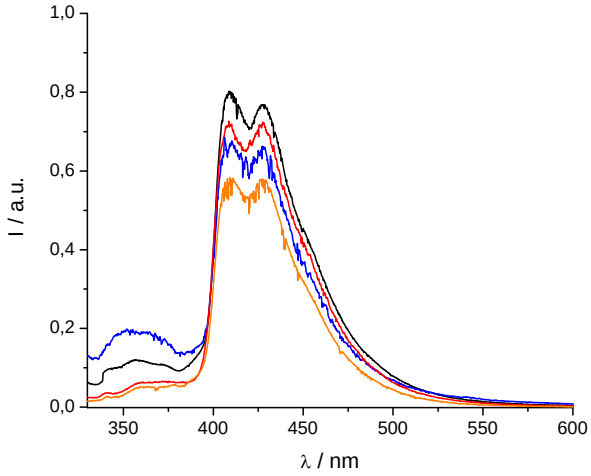

Figure 2.

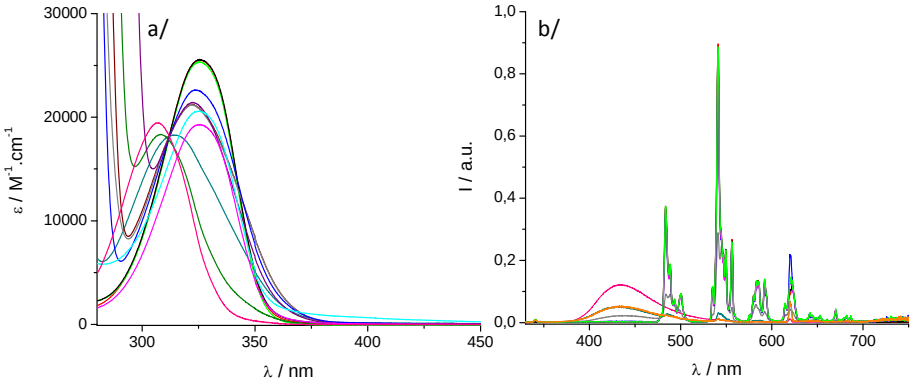

Figure 3.

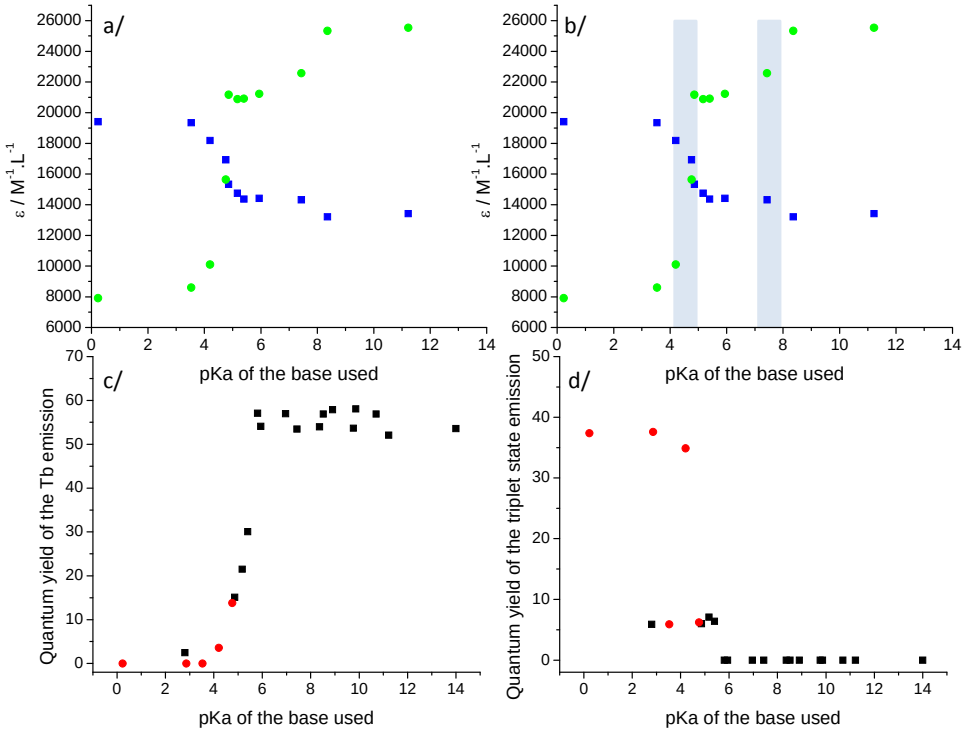

Figure 4.

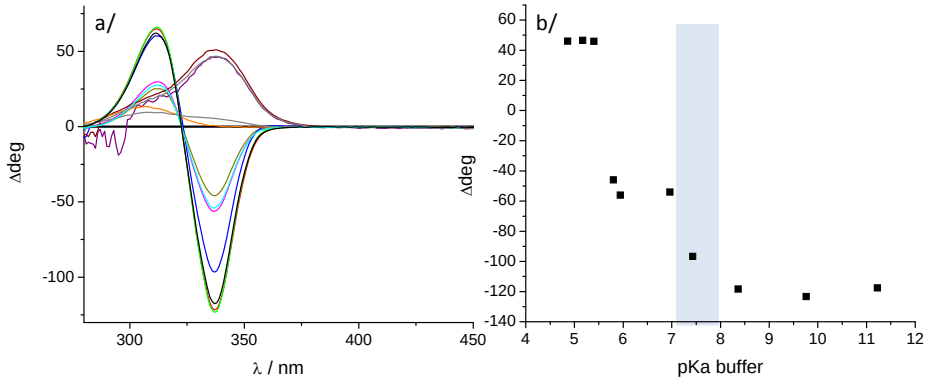

Figure 5.

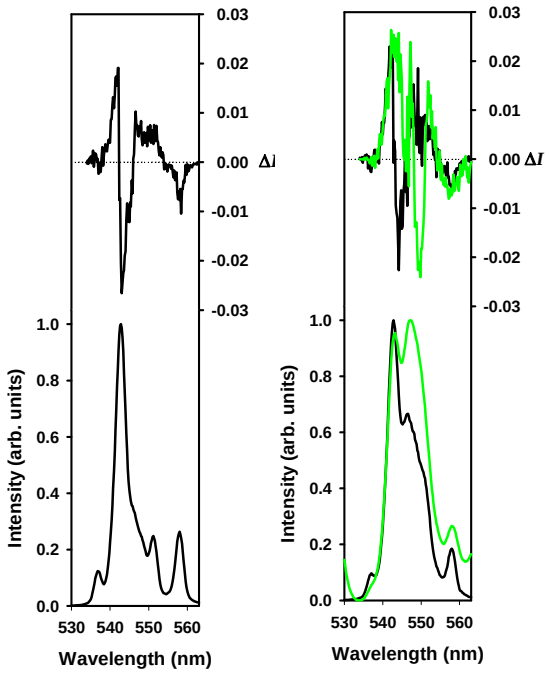

Figure 6.

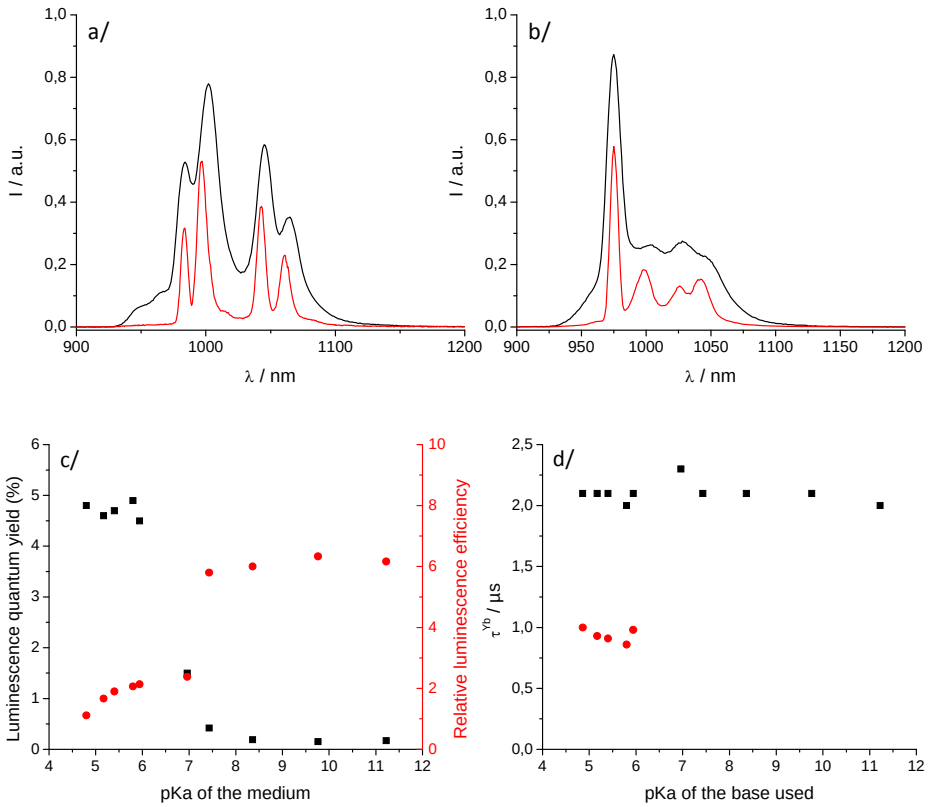

Figure 7.

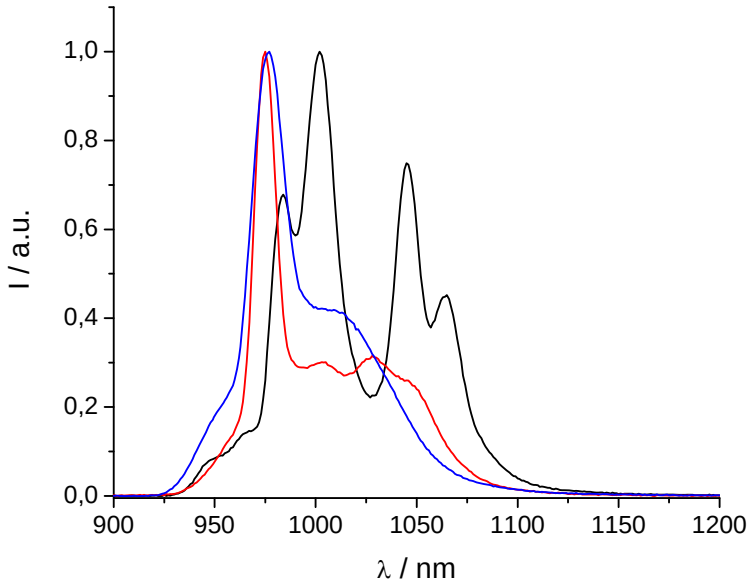

Figure 8.

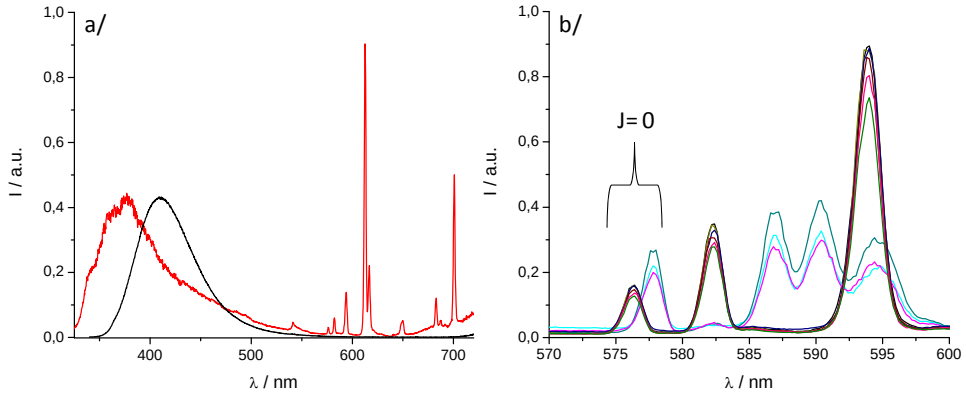

Figure 9.

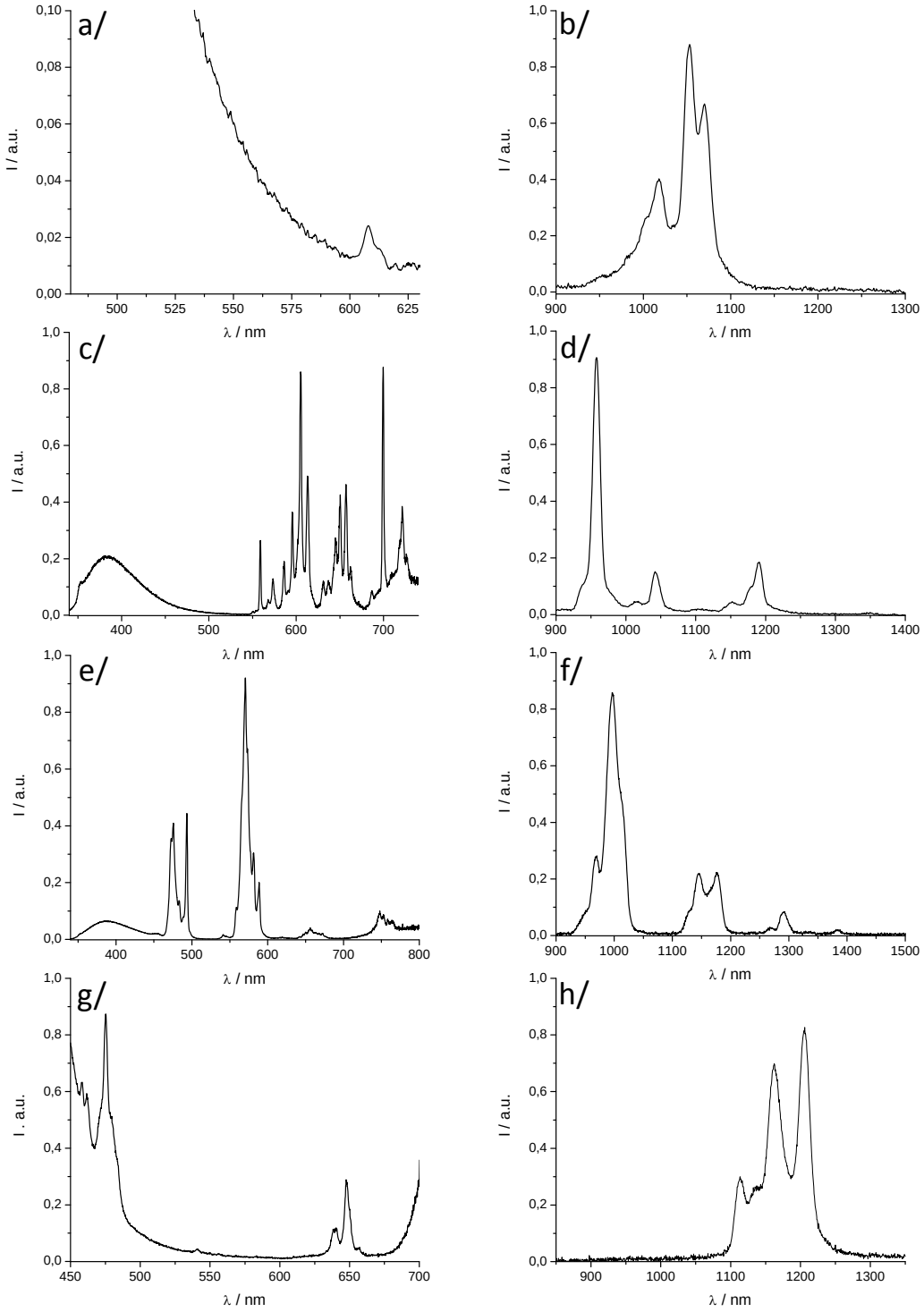

Figure 10.